11th World Congress on Computational Mechanics (WCCM XI)
5th European Conference on Computational Mechanics (ECCM V)
6th European Conference on Computational Fluid Dynamics (ECFD VI)
E. Oñate, J. Oliver and A. Huerta (Eds)

SIMULATION OF BIAXIAL FATIGUE CRACK GROWTH IN VARIOUS MICROSTRUCTURES MODELLED BY USING VORONOI-POLYGONS

YUTA HITOTSUGI[*] AND TOSHIHIKO HOSHIDE[†]

[*] Department of Energy Conversion Science, Graduate School of Energy Science, Kyoto University
Yoshida-Honmachi, Sakyo-ku, Kyoto, 606-8501, Kyoto, Japan
e-mail: hitotsugi.yuuta.25w@st.kyoto-u.ac.jp

[†]Department of Energy Conversion Science, Graduate School of Energy Science, Kyoto University
Yoshida-Honmachi, Sakyo-ku, Kyoto, 606-8501, Kyoto, Japan
e-mail: hoshide.toshihiko.5c@kyoto-u.ac.jp

Key Words: *Simulation, Biaxial fatigue, Microstructure, Voronoi-polygon.*

Abstract. In this work, a modelling procedure was developed so that it should be applicable to the analysis of crack growth in materials with various microstructures under biaxial fatigue. In the modelling, microstructures of two different polycrystalline materials were modelled by using Voronoi-polygons. Then, the crack initiation was analysed as the slip plane separation in an individual grain, and the number of cycles required for the separation was calculated by using a dislocation pile-up model. In the crack propagation stage, the crack growth was analysed as a competition between the growth by crack linkage during crack initiation and propagation stages and the propagation of a dominant crack as a single crack.

The simulated cracking morphologies and the resultant lives were compared with experimental results observed in biaxial fatigue tests, which had been conducted by using two titanium alloys having different microstructures. The comparison revealed that the simulated results almost correspond with experimental results.

1 INTRODUCTION

The majority of failures in structural or functional systems are caused by fatigue. So when we intend to design structural or functional systems with long term durability, fatigue experiments under various conditions are needed to ensure that fatigue does not occur in such systems. By considering difficulty in conducting experiments under various conditions, simulation procedures are required in order to adequately describe crack growth behaviour, which determines fatigue life.

It is recognized that crack growth in low cycle fatigue is affected by two factors; i.e., material microstructure and stress state [1,2]. From this point of view, simulation procedures are developed so that they could describe influence of microstructure and biaxial stress state on crack growth [3-7]. It is still at issue, however, that previous models of material microstructure used in the simulation bring uniform grain-structures and do not properly

represent non-uniform microstructures as seen in real materials.

In this work, an updated analytical procedure is developed based on previous model [8] so that it should be applicable to biaxial fatigue behaviour in materials with non-homogeneous microstructures. Modelling of microstructure in a polycrystalline material is especially improved in this investigation, and a microstructure is modelled by using Voronoi-polygons. Numerical simulations using the proposed model were conducted to investigate the microstructural effects on crack growth in materials with different microstructures under axial, torsional and combined axial-torsional loading modes. The simulated cracking morphologies and the resultant lives were compared with experimental results observed in biaxial fatigue tests, and the applicability of the proposed model was discussed.

2 TWO-DIMENSIONAL MODELLING OF POLYCRYSTALLINE MATERIALS

2.1 Materials to be modelled

Materials to be analysed in this simulation are an (α+β) and a β titanium (Ti) alloy. The microstructures of each material are presented in Figure 1. The two Ti-alloys have the same chemical composition, i.e. 6.52 wt. % Al, 4.00 wt. % V, 0.18 wt. % O, 0.16 wt. % Fe, and other elements less than 0.01 wt. %. They have been produced by different heat-treatment and processing histories, so a remarkable difference in microstructure is observed between the two Ti-alloys. A quasi-isotropic microstructure is found in the β Ti-alloy, while grains in the (α+β) Ti-alloy are stretched in the axial direction. As for the (α+β) Ti-alloy, the average aspect ratio and the mean size of stretched α-grains, which were preferable sites for crack initiation, are approximately 2 and 8.5 μm, respectively. Contrarily, the mean grain-size in the β Ti-alloy is very huge, i.e. 400 μm.

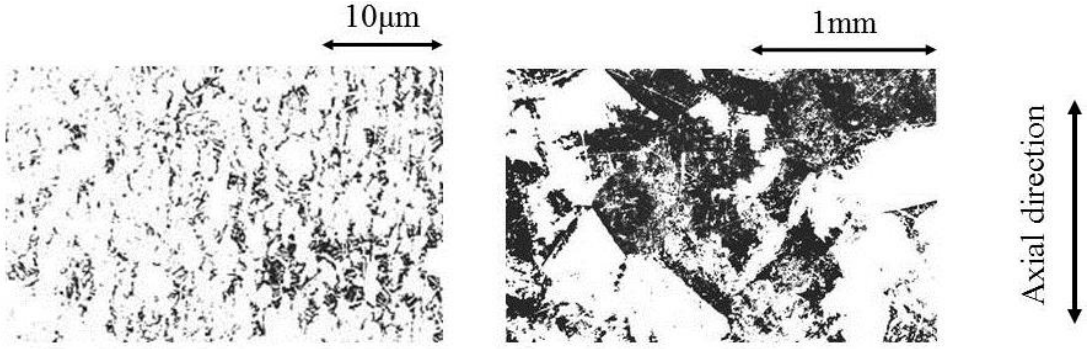

(a) (α+β) Ti-alloy (b) β Ti-alloy

Figure 1: Microstructures of the simulated materials

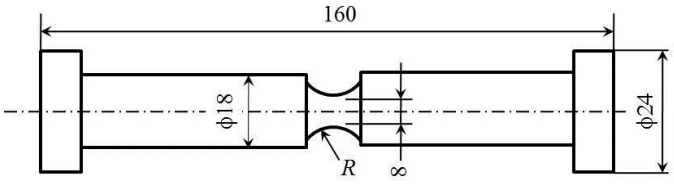

Figure 2: Dimensions of the notched specimens

Specimens are of a solid cylindrical type with a circumferential blunt notch of root radius R = 6 mm, as shown in Figure 2. The fatigue behaviour of these materials has been investigated experimentally in other works [9].

2.2 Modelling of microstructures by using Voronoi-polygons

In this work, a solid cylindrical specimen is considered, and a cylindrical coordinate system r–θ–z is introduced, where r–, θ– and z–axes coincide respectively with radial, circumferential and axial directions in the specimen.

The microstructure on the surface of a cylindrical specimen is modelled as a two-dimensional area by using Voronoi-polygons. A Voronoi diagram is a kind of decomposition of a metric space, which is determined by distances to a specified discrete set of points in the space [10]. It is also known that an aggregate of convex hexagons is obtained as Voronoi-polygons in a two-dimensional area. The merit in adopting Voronoi-polygons for microstructure of polycrystalline material is that a modelling of microstructure is possible under a simple algorithm in numerical analysis.

A curved surface on solid cylindrical specimen, where fatigue cracks grow, is developed into a flat surface. This implies that the circumferential direction (θ–direction) of a specimen is developed onto the horizontal direction in the two-dimensional surface when the specimen axis (z–direction) is set to coincide with the vertical direction. The size of the aforementioned two-dimensional area may be changed depending on material microstructure, specimen geometry under consideration and convenience of conducting analysis.

The number of polygons in the analysed area is determined so that the resultant mean grain-size should approximately equal the size measured in experiment. The polygon-number for a material consisting of one phase is determined by the just-above mentioned procedure. On the other hand, in a material having the second phase, Voronoi-polygons are randomly selected among all Voronoi-polygons so that an area-ratio of selected polygons occupying in the analysed area could coincide with the phase composition observed in the material microstructure. When a material to be modelled has grains stretched in the axial direction as seen in (α+β) Ti-alloy and stretched grains have the average aspect ratio λ, the axial length of an area modelled by ordinary Voronoi-polygons will be multiplied by λ.

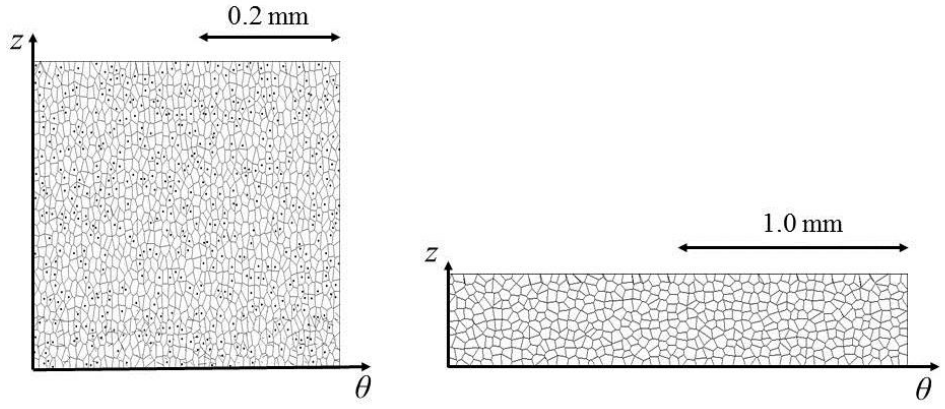

(a) (α+β) Ti-alloy (b) β Ti-alloy

Figure 3: Modelled microstructures

Polygons formed as mentioned above are hereafter called grains, which constitute a polycrystalline material. Figure 3 presents examples of modeled microstructures, which are depicted by modelling two different microstructures. Grains with black-points in themselves in the (α+β) Ti-alloy represent β grains.

3 MODELLING FOR FATIGUE CRACK GROWTH

A competition model for crack growth established by the authors [3,4] is also applied in this simulation. The model postulates that the cracking morphology and the fatigue failure life are determined as a result of competition between the growth by crack coalescence and the propagation of a dominant crack as a single crack. The competition implies that the dominant crack growth will be governed by the faster growth mode. Figure 4 presents the outline of the present simulation. The analytical procedure for each mode is summarized as follows.

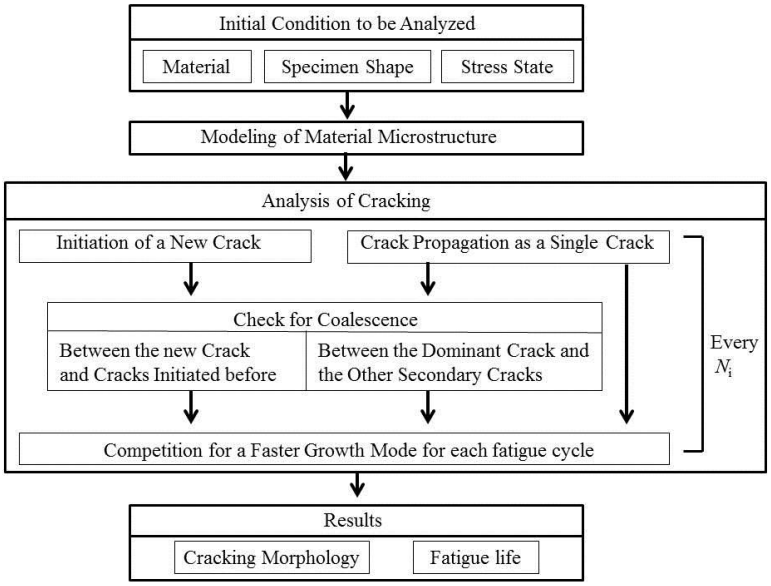

Figure 4: Flowchart of the analytical procedure

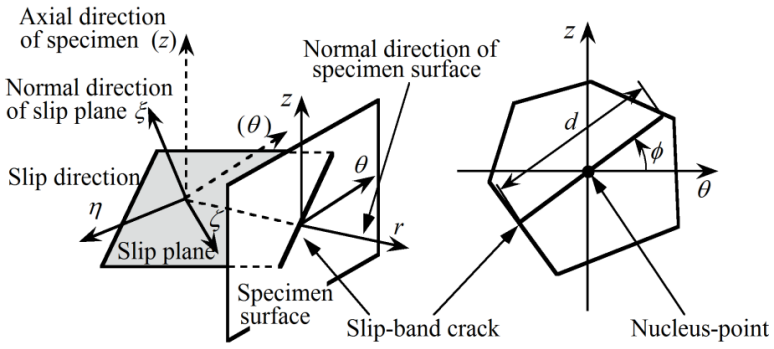

Figure 5: Coordinate systems related with slip plane and angle of slip-band

3.1 Crack initiation analysis

In the crack initiation analysis, the r–θ–z coordinate system is employed as depicted in Figure 5. The z–axis is set to be parallel to the axial direction of specimen. Consider a slip plane in one grain on the specimen surface. On the slip plane, another orthogonal ξ–η–ζ coordinate system is also defined so that ξ– and η– axes should be respectively parallel to the normal direction of the slip plane and the slip direction on the slip plane.

The stress tensor $[\sigma_{\xi\eta\zeta}]$ for the slip system is correlated with an applied stress tensor $[\sigma_{r\theta z}]$ in the following. At first, a directional cosine tensor $[l]$ is introduced, and is used for the transformation between r–θ–z and ξ–η–ζ coordinates. By using the directional cosine tensor $[l]$, the stress tensor $[\sigma_{\xi\eta\zeta}]$ for the slip system is calculated by Eq. (1) in the material subjected to the applied stress tensor $[\sigma_{r\theta z}]$.

$$[\sigma_{\xi\eta\zeta}] = [\, l \,]\, [\sigma_{r\theta z}]\, [\, l \,]^{\mathrm{T}} \tag{1}$$

The superscript "T" in the above equation represents the transposed matrix, and components in the stress tensors are given as follows.

$$[\sigma_{r\theta z}] = \begin{bmatrix} \sigma_r & \tau_{r\theta} & \tau_{rz} \\ \tau_{\theta r} & \sigma_\theta & \tau_{\theta z} \\ \tau_{zr} & \tau_{z\theta} & \sigma_z \end{bmatrix}, \text{ and } [\sigma_{\xi\eta\zeta}] = \begin{bmatrix} \sigma_\xi & \tau_{\xi\eta} & \tau_{\zeta\xi} \\ \tau_{\xi\eta} & \sigma_\eta & \tau_{\eta\zeta} \\ \tau_{\zeta\xi} & \tau_{\eta\zeta} & \sigma_\zeta \end{bmatrix} \tag{2}$$

The directional cosine tensor $[l]$ is expressed as Eq. (3)

$$[\, l \,] = \begin{bmatrix} l_{r\xi} & l_{r\eta} & l_{r\zeta} \\ l_{\theta\xi} & l_{\theta\eta} & l_{\theta\zeta} \\ l_{z\xi} & l_{z\eta} & l_{z\zeta} \end{bmatrix} \tag{3}$$

The components of $[l]$ are defined between r–θ–z and ξ–η–ζ coordinates as shown in Table 1.

Table 1: Directional cosines between r–θ–z and ξ–η–ζ coordinates

Axes	ξ	η	ζ
r	$l_{r\xi}$	$l_{r\eta}$	$l_{r\zeta}$
θ	$l_{\theta\xi}$	$l_{\theta\eta}$	$l_{\theta\zeta}$
z	$l_{z\xi}$	$l_{z\eta}$	$l_{z\zeta}$

Considering slip in a surface grain, we may assume the plane stress state, i.e., $\sigma_r = \tau_{rz} = \tau_{zr} = \tau_{r\theta} = \tau_{\theta r} = 0$. Under the above assumption, the resolved shear stress $\tau_{\xi\eta}$ in the slip direction on the associated slip plane, which is one of the most important factors for the feasibility to slip, is represented by

$$\tau_{\xi\eta} = \sigma_z\, l_{z\eta}\, l_{\theta\eta} + \sigma_\theta\, l_{z\xi}\, l_{\theta\xi} + \tau_{z\theta}\,(l_{z\xi}\, l_{\theta\eta} + l_{z\eta}\, l_{\theta\xi}) \tag{4}$$

In this model, it is assumed that a slip-band becomes a transgranular crack along the slip-band when the criterion of Eq. (5) is satisfied and the number of stress cycles, N_{i}, which is required to make a slip-band into a crack, has passed.

$$\tau_{\xi\eta} > \tau_{\mathrm{c}} \tag{5}$$

In the above equation, $\tau_{\xi\eta}$ is given by Eq. (4) and τ_c is the critical shear stress to make a slip active. The number of stress cycles, N_i, is identical to the crack initiation life, and is calculated by using a dislocation pile-up model [11] as follows

$$N_i = \frac{2GW_c}{\pi(1-\nu)d(\tau_{\xi\eta}-\tau_c)^2} \tag{6}$$

Parameters G, ν and W_c in Eq. (6) are respectively the shear elastic modulus, Poisson's ratio and the fracture surface-energy, all of which are material constants. A parameter d in Eq. (6) is the slip-band length in a grain to be considered in the slip analysis, and is equivalent to a length of crack initiated in the grain.

3.2 Crack propagation analysis

The mode of crack propagation is analysed assuming that the growth rate da/dN is described by a power function of the J-integral range ΔJ as

$$\frac{\mathrm{d}a}{\mathrm{d}N} = C(\Delta J)^m \tag{7}$$

where C and m are the coefficient in crack growth low and the exponent in the crack growth law. The J-integral range for short cracks is evaluated as follows [12,13]:

$$\Delta J = 2\pi M_J \Delta W a \tag{8}$$

where a is the half length of surface crack.

For the mode I crack, $M_J = (M_K/\Phi)^2\lambda$, where M_K is the geometric correction factor for the stress intensity factor of the crack under consideration, Φ is the complete elliptic integral of the second kind and λ is the crack aspect ratio. The energy density parameter ΔW is given as

$$\Delta W = \frac{\Delta\sigma^2}{2E} + f(n')\frac{\Delta\sigma\,\Delta\varepsilon^p}{1+n'} \tag{9}$$

with

$$f(n') = \frac{1+n'}{2\pi}\left[\frac{3.85(1-n')}{\sqrt{n'}} + \pi n'\right] \tag{10}$$

where $\Delta\sigma$, $\Delta\varepsilon^p$, E and n' are the nominal stress range, the nominal plastic strain range, Young's modulus and the exponent of cyclic strain hardening, respectively.

3.3 Crack coalescence analysis

In this section, two modes of crack coalescence are described, and a mean grain-size D of a material is employed as a reference size parameter in coalescence criterions.

During the crack initiation stage, the coalescence growth is taken into account among the distributed cracks for which initiation lives are calculated by Eq. (6). A crack under consideration is assumed to link with one of the other initiated cracks, if the tip-to-tip distance between the cracks is less than a specific length ξD. This algorithm gives us quantitative information for the crack growth by linkage mode in the crack initiation stage.

The crack coalescence analysis is also carried out during the propagation stage of a dominant crack. In the analysis, coalescence is assumed to occur when the distance between the tips of the dominant crack and the other secondary or initiated cracks is less than a specific length ζD.

Each coalescence criterion is checked at the number of cycles when a new crack is initiated in the analysis. The values of ξ and ζ, which depend on the microstructure and the loading mode, are determined according to experimental observations. Crack linkage occurs more easily for larger values of ξ and ζ.

4 SIMULATED RESULTS AND DISCUSSIONS

4.1 Parameters used in the simulation and the simulation procedures

Material constants used in the simulation for each material are summarized in Table 2. The constants C and m in Eq. (7) are obtained for da/dN in m/cycle and ΔJ in N/m. The parameters ξ and ζ associated with crack coalescence analyses have been determined based on actual crack coalescence behaviour, which was observed on sequential plastic replicas taken on specimen surfaces during fatigue tests for each material.

Table 2: List of parameters used in the simulation

Parameters	(α+β) Ti-alloy	β Ti-alloy
E (MPa)	110	127
G (GPa)	41	45
v	0.35	0.41
W_c (kJ/m^2)	2.0	2.0
τ_c (MPa)	288	296
C	1.07×10^{-10} (axial)	7.03×10^{-12} (axial)
	1.10×10^{-10} (combined)	1.89×10^{-10} (combined)
	3.91×10^{-15} (torsional)	3.86×10^{-11} (torsional)
m	1.12 (axial)	1.32 (axial)
	0.96 (combined)	0.84 (combined)
	1.74 (torsional)	0.82 (torsional)
ξ	1.0 (axial, combined)	1.0 (axial, combined)
	4.0 (torsional)	1.6 (torsional)
ζ	1.0 (axial, combined)	1.0 (axial, combined)
	4.0 (torsional)	1.6 (torsional)

Fatigue test conditions to be simulated are fully reserved and load-controlled conditions in axial, torsional and combined axial-torsional modes [9]. In the combined loading mode, the ratio of elastic nominal stress to shear range, $\Delta\sigma_z / \Delta\tau_{z\theta}$, was set to $3^{1/2}$. Equivalent stress ranges tested in the experiments were respectively 2200, 2000 and 1800 MPa in the (α+β) Ti-alloy, and 2100, 1900 and 1700 MPa in the β Ti-alloy. The experiments revealed that the cyclic deformation characteristics of each material were more appropriately described by using the equivalent stress and strain of von Mises type.

Computer simulations for the fatigue testing conditions specified for each material were carried out using a statistical procedure of Monte Carlo type. Employing 50 series of uniform random numbers, 50 distinct modelled microstructures are generated for each material. They are composed of differently shaped grains with a variation in the direction of slip-lines. This

results in 50 distinct cracking patterns and their corresponding fatigue lives for a given testing condition for each material.

4.2 Cracking morphology

Typical examples of simulated morphologies of dominant cracks and other secondary cracks in an analysed area are illustrated in Figure 6, where the dominant cracks are drawn with bold lines. Figure 7 shows the cracking behaviour observed in the experiments [9]. By comparing the simulated and experimental cracking patterns, it is found that the simulated morphologies of dominant cracks almost coincide with those observed in the experiments.

From a macroscopic aspect, the growth direction of a dominant crack in the case of the axial and combined loading almost coincides with the direction vertical to the maximum principal stress direction for both of the materials. However, in the torsional loading, the macroscopic growth direction of a dominant crack is found to be affected by the microstructures as follows. In the (α+β) Ti-alloy with stretched α-grains, the growth direction of a dominant crack is parallel to the axial direction. This behaviour is supposed to be caused by an anisotropic microstructure. On the other hand, in the β Ti-alloy having very large grains compared with those of (α+β) Ti-alloy, the growth direction of a dominant crack almost coincides with the direction vertical to the maximum principal stress direction.

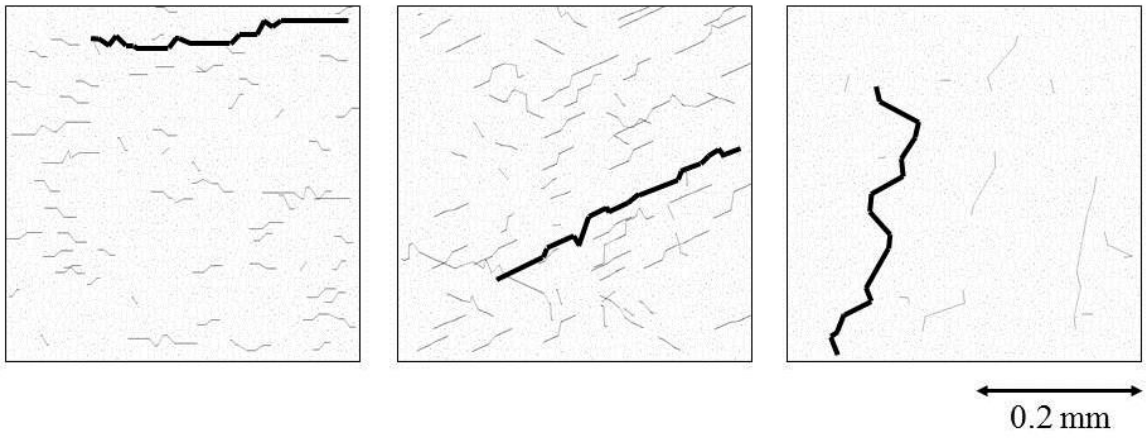

(a) (α+β) Ti-alloy

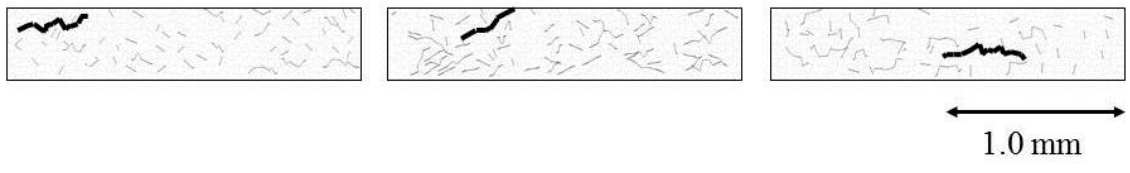

(b) β Ti-alloy

Figure 6: Simulated cracking morphologies

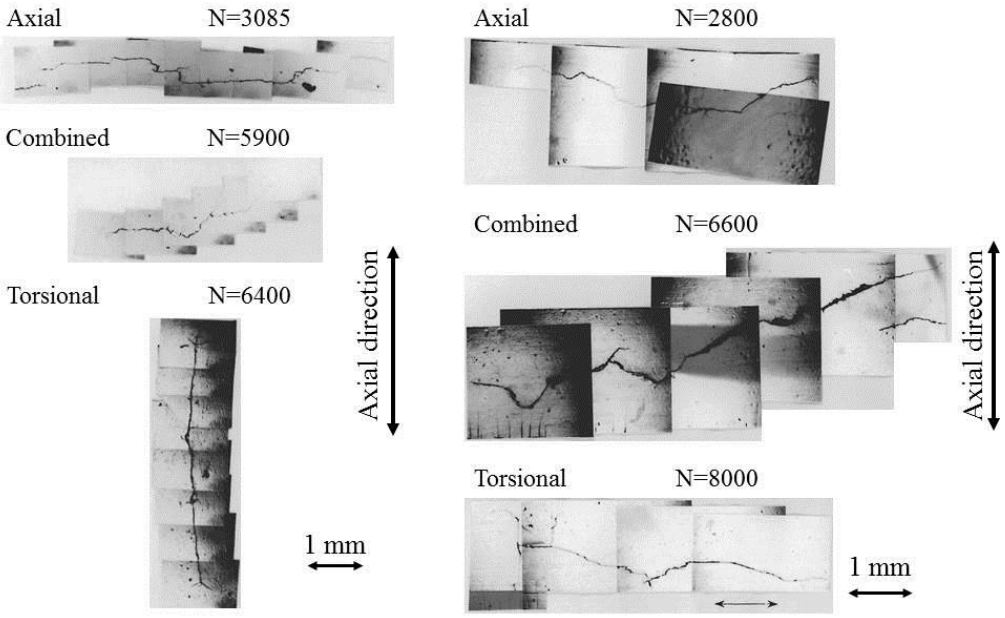

(a) (α+β) Ti-alloy (b) β Ti-alloy

Figure 7: Cracking morphologies observed in experiments

4.3 Failure life

The failure life N_f in experiments is defined as the number of cycles at which a dominant crack of specific length is formed in the notched zone. The specific length for each material is determined according to experimental observations as follows [9]; 0.3 mm for the (α+β) Ti-alloy and 3 mm for the β Ti-alloy.

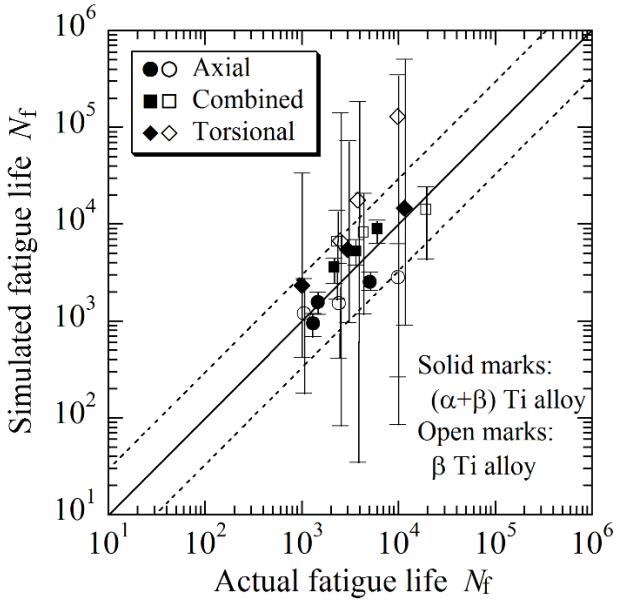

Figure 8: Comparison between experimental and simulated fatigue lives

Figure 8 shows a comparison between experimental and simulated lives. The simulated lives are calculated as the number of cycles, at which the length of a dominant crack reaches the same length as that obtained in the experiment. In the figure, each mark presents the actual fatigue life correlated with the average of 50 lives simulated for each material under respective loading condition. Two dotted lines are drawn in Figure 8 to indicate a variation band-range of factor of three. It is found that almost all marks are included in the band-range, excepting the result of β Ti alloy subjected to torsional loading under the lowest applied stress. Consequently, it may be concluded that the proposed procedure is applicable to the prediction of fatigue life variation within a factor of three.

In the simulation, 50 simulated lives are obtained, so some statistical discussion may be possible. An error-bar in Figure 8 shows a life variation ranging from the simulated minimum to maximum lives. As seen in Figure 8, the dispersion of simulated fatigue life is largest under torsional loading for the both materials. The life dispersion in β Ti alloy is larger than that in (α+β) Ti alloy. In β Ti alloy, especially, the size of cracks initiated in grains becomes larger corresponding to huge grain-size. Therefore, the fatigue life is significantly affected by the frequency of crack coalescence. When the crack coalescence frequently occurs, the fatigue life may be reduced because it is defined as the number of cycles at which the length of a dominant crack reaches a specified length.

5 CONCLUSIONS

In the present work, a modelling procedure of fatigue crack growth was developed in the following way. At first, microstructures of polycrystalline materials were modelled by using Voronoi-polygons. Especially for a microstructure having stretched grains, a modified procedure was established adequately to represent such an unordinary microstructure. Then, the crack initiation was analysed as the slip plane separation in an individual grain and the number of cycles required for the separation was calculated by using a dislocation pile-up model. In the crack propagation stage, the crack growth was analysed as a competition between the growth by crack linkage during crack initiation and propagation stages and the propagation of a dominant crack as a single crack.

By using a procedure proposed in this work, simulations of Monte Carlo type were carried out for two titanium alloys with different microstructures. The simulated cracking morphologies and resultant fatigue lives were compared with experimental results observed in biaxial fatigue tests of the two titanium alloys. It was clarified that simulated life ranges almost covered experimental results.

It may be concluded that the proposed procedure using Voronoi-polygons in modelling microstructure is applicable to the analysis of fatigue crack growth affected by microstructural variation and stress state.

REFERENCES

[1] Hua, C. T. and Socie, D. F. Fatigue damage in 1045 steel under variable amplitude biaxial loading. *Fatigue Fract. Engng Mater. Struct.* (1985) **8**: 101-114.

[2] Bannatine, J. A. and Socie, D. F. Observations of cracking behavior in tension and torsion low cycle fatigue. *ASTM STP* (1988) **942**: 899-921.

[3] Hoshide, T. and Socie, D.F. Crack nucleation and growth modeling in biaxial fatigue. *Engng Fract. Mech.* (1988) **29**: 287-299.
[4] Hoshide, T., Kawabata, T. and Inoue, T. Analysis of intergranular cracking in low cycle fatigue under biaxial stress. *Trans. Jpn Soc. Mech. Engnr, Ser. A* (1989) **55**: 222-230.
[5] Hoshide, T., Yokota, K. and Inoue, T. Investigation on small crack growth and life properties in fatigue of circumferentially-notched component of pure copper subjected to combined loading. *J. Soc. Mater. Sci. Jpn* (1990) **39**: 144-149.
[6] Argence, T., Weiss, J. and Pineau, A. Observation and modelling of transgranular and intergranular multiaxial low-cycle fatigue damage of austentic stainless steels. *Multiaxial Fatigue Design, ESIS 21* (Edited by Pineau, A., Gailetaud, G. and Lindley, T. C.). Mechanical Engineering Publications, Bury St Edmunds, U.K., Vol. IV (1996): 209-227.
[7] Socie, D. F. and Furman, S. Fatigue damage simulation models for multiaxial loading. *Proc. 6th Int. Conf. on Fatigue Congress*, *FATIGUE '96* (Edited by Lütjering, G. and Nowack, H.). Elsevier Science, Oxford, U.K., Vol. II (1996): 967-976.
[8] Hoshide, T. and Kusuura, K. Life prediction by simulation of crack growth in notched components with different microstructures and under multiaxial fatigue. *Fatigue Fract. Eng. Mater. Struct.* (1998), **21**: No. 2, 201-213.
[9] Hoshide, T., Hirota, T. and Inoue, T. Fatigue behaviour in notched component of (α+β) and β titanium alloys under combined axial-torsional loading. *Mater. Sci. Res. Int.* (1995) **1**: 169-174.
[10] Okabe, A., Boots, B., Sugihara, K. and Chiu, S.N. *Spatial Tessellations – Concepts and applications of Voronoi Diagrams.* John Wiley, Chichester, 2nd ed. (2000).
[11] Tanaka, K. and Mura, T. A dislocation model for fatigue crack initiation. *Trans. ASME, J. Appl. Mech.* (1981) **48**: 97-103.
[12] Hoshide, T., Yamada, T., Fujimura, S. and Hayashi, T. Short crack growth and life prediction in low-cycle fatigue of smooth specimens. *Engng Fract. Mech.* (1985) **21**: 85-101.
[13] Hoshide, T. and Socie, D. F. Mechanics of mixed mode small fatigue crack growth. *Engng Fract. Mech.* (1987) **26**: 841-850.